International Journal of Gas Turbine, Propulsion and Power Systems
December 2013, Volume 5, Number 1

Multi-Objective Optimization of Three-Dimensional Blade Shape for an Axial Compressor Rotor in Transonic Stage

Chihiro Myoren[1], Yasuo Takahashi[1] and Yasuhiro Kato[1]

[1] Hitachi Laboratory, Hitachi, Ltd.
7-1-1 Omika-cho, Hitachi-shi, 319-1221, JAPAN
E-mail: chihiro.myoren.uc@hitachi.com

ABSTRACT

A three-dimensional (3D) blade design method for an axial compressor transonic stage to optimize the aerodynamic performance is presented in this paper. The blade is defined by three profiles and a radial stacking line. Each profile is a multi circular arc (MCA), and the stacking line is defined as a B-spline curve with six design parameters. To ensure the off-design performance, a multi-objective genetic algorithm (MOGA) is applied. The objective functions are the efficiency, shock position and leading edge pressure difference at the design point. Because shock position and leading edge pressure difference can evaluate the potential for stalling, the method can generate blades with a wide operating range with just one performance prediction. This method is applied in a transonic blade design. The result shows that the efficiency of the optimized blade at the design point is increased and the operation range is expanded compared with the original blade.

NOMENCLATURE

C	Chord length [mm]
DPL	Normalized pressure difference at leading edge [-]
G	Mass flow rate [kg/s]
H	Blade height [mm]
i	Incidence angle [deg]
Pt	Total pressure [MPa]
S	Slope of stacking line [-]
Tt	Total temperature [degC]
X	Axial coordinate [mm]
Xm	Maximum thickness position [%]
Xc	Combination position of arcs [%]
Xs	Shock position [%]
Y	Circumferential coordinate [mm]
γ	Specific heat ratio [-]
η	Efficiency [%]
π	Pressure ratio [-]
θ	Central angle of arc [deg]
σ_c	Centrifugal stress [MPa]
σ_g	Gas bending stress [MPa]

-Subscripts-

1	Inlet of the cascade
2	Outlet of the cascade
d	Design point
h	Blade hub
t	Blade tip

Presented at International Gas Turbine Congress 2011 Osaka, November 13-18, Osaka, Japan, IGTC2011-0055
Review completed on December 25, 2013

INTRODUCTION

In recent years, use of highly loaded axial compressor blades with high efficiency is essential to achieve both performance improvement and cost reduction. To apply these blades for transonic stages, the shock wave on the blade surface should be alleviated because a high load causes stronger shock wave. For reduction of shock loss, control diffusion airfoils and 3D blades were developed. These performances were studied in detail by Denton and Xu (2002) and Bonaiuti et al. (2007). Recently, Iwatani et al. (2007) and Zheng et al. (2010) studied the performance of a sweep blade, which was a kind of 3D blades. They showed that an S-shaped stacking line could reduce the shock loss. However, adopting sweep blades will increase the total design time because more design parameters are needed than for conventional blades.

To reduce design time, a lot of researchers have carried out optimization of 3D blades using computational fluid dynamics (CFD). In these studies, multi-objective optimizations were used in order to achieve more than two design goals. For example, Li et al. (2006) applied a new geometry deformation approach called ‘aerodynamic mode shape’ in an aero-mechanical optimization to reduce the number of design parameters. Luo et al. (2009) used the Multi-objective Differential Evolution (MDE) algorithm as an optimizer to find the Pareto solutions of an aero-mechanical problem easily. However, most of the design goals of these researchers were usually for aerodynamic performance at the design point, blade stress and vibration. Few researchers have used aerodynamic performance at off-design points as the design goal of the optimization, because additional performance calculations at off-design points should be carried out.

In this paper, a 3D blade design method to optimize the aerodynamic performance at both the design point and off-design points by only one calculation at the design point is presented. This method is applied in an aerodynamic design of a blade, for which specifications are almost the same as the first stage rotor of a conventional axial compressor. To validate the method, optimized blades are compared with a blade optimized by the method just with an objective function related to the performance at the design point.

THREE-DIMENSIONAL BLADE DESIGN SYSTEM

Flow diagram

The flow diagram of the developed system is shown in fig.1. In this system, the optimization procedure consists of the blade definition, structural analysis, flow analysis, and evaluation of the objective functions by the optimization algorithm. All the processes are done using the optimization support program modeFRONTIER 4.2.0. The optimization is finished when the generation number N reaches the maximum generation number Nmax defined in advance.

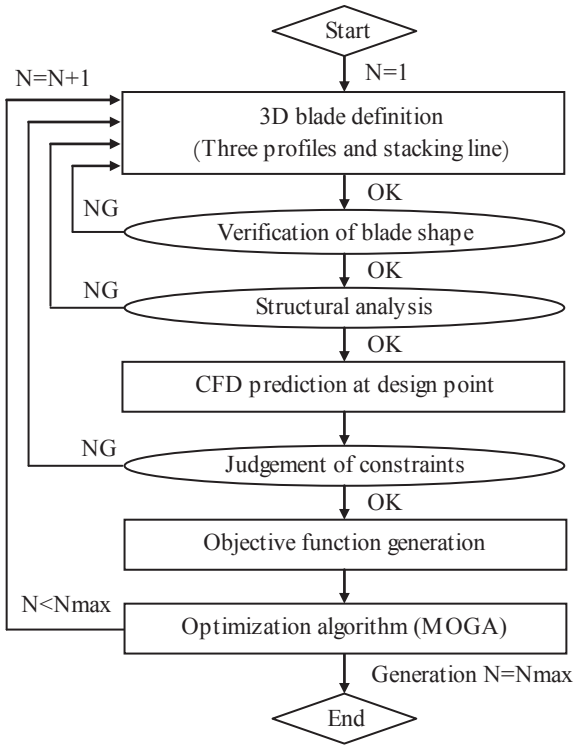

Fig.1 Flow diagram of the developed system

Blade parameterization

In this system, the shape of the 3D blade is defined by the combination of profiles and stacking line. Fig.2 shows the definition of the blade shape. Profiles of the blade are defined at three radial positions, that is, hub, mean, and tip section of the blade. Profiles at the other radial positions are calculated by the interpolation.

On the other hand, the stacking line is defined as a 4th order non-uniform B-spline curve including four control points and two slopes at the blade hub and tip. The direction of the movement of the control points is the same as the blade stagger angle, in order to design sweep blades which may be effective for shock loss reduction. Since the meridional flow path is maintained in the system when making a sweep blade, the tip diameter of the blade is changed to follow the flow path.

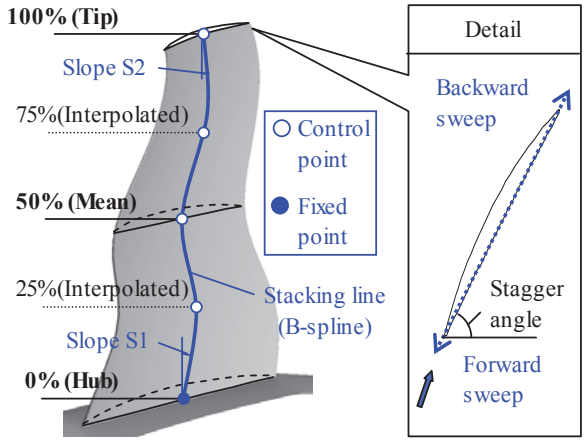

Fig.2 Definition of the blade shape

Fig.3 shows details of design parameters of the profile. The MCA, which has suction and pressure surfaces consisting of two circular arcs, is applied for the profile. Its definition parameters are the incidence angle, the position of the maximum thickness, the combination position of two arcs of blade surface, and the ratio of two camber central angles. Since some combinations of the parameters may generate profiles without enough blade thickness near leading and trailing edges, preliminary estimations of the range of the parameters keeping a desirable blade thickness are included in the system to reduce calculations of such unnecessary cases.

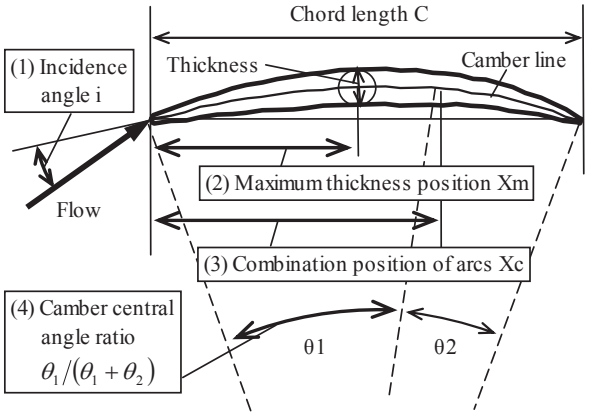

Fig.3 Details of design parameters of a profile

Optimization method and objective functions

The system optimizes performances at both the design point and off-design points using just one calculation result at the design point. Therefore, indexes are included in the system to estimate the off-design point performance by the calculation at the design point. Details of the indexes are shown in Fig.4 and 5. Fig.4 is an example of the flow characteristic of efficiency of a transonic blade, and Fig.5 is a conceptual diagram of flow field of a transonic blade at near the stall point.

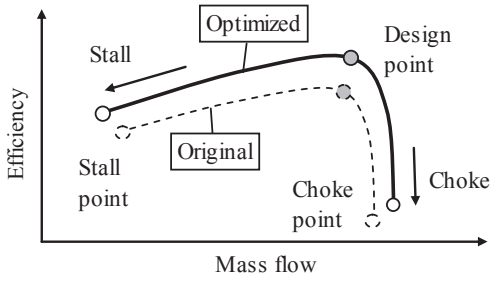

Fig.4 Example of flow characteristic of efficiency of a transonic blade

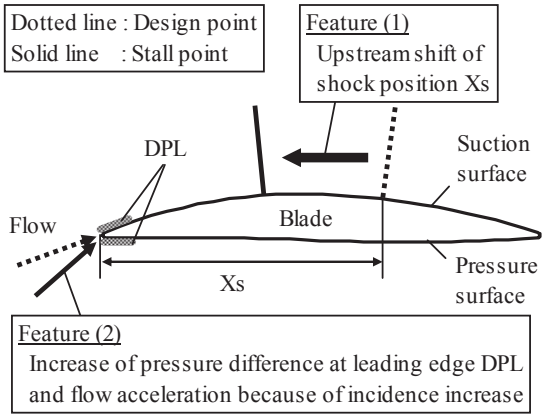

Fig.5 Conceptual diagram of flow field of a transonic blade at near stall point

Like the characteristic in Fig.4, the performance of the optimized blade at all operating points should be better than the original blade by optimization of the system. At off-design points near the choke point, at which the mass flow rate becomes the maximum value, the efficiency is mainly determined by the strength of shock wave. Since this indicates that shock reduction at the design point leads to enhanced efficiency at off-design points near the choke point, there is no index to estimate the off-design performance near the choke point in the system.

On the other hand, the system needs indexes at off-design points near the stall point, at which the mass flow rate becomes the minimum value. When the operating point changes from the design point near the stall point, there are two important changes in the flow field of the blade. The first one is the increase of the pressure difference between the suction surface and pressure surface near the leading edge, and the other one is the shift of the shock wave toward the inlet. Either of them has an effect on the flow separation and the blade might encounter a stall. To avoid flow separation, the shock position Xs and pressure difference between the suction surface and pressure surface near the leading edge DPL at the design point are introduced as indexes in the system. However, the importance of the two indexes for the flow separation depends on the span-wise position. Therefore, Xs and DPL are defined as the weight averages of span-wise position as written in Eqs.(1) and (2).

$$Xs = \sum_{k=1}^{5} \alpha_k Xs_k \tag{1}$$

$$DPL = \sum_{k=1}^{5} \beta_k DPL_k \tag{2}$$

In Eqs.(1) and (2), k means the number of span-wise positions, and α and β are the weights for each index. Table.1 shows details of k, α and β. In table.1, the span-wise positions of α and β at the hub and tip are defined at the 5% and 95% span so as to avoid the effect of endwall boundary layer. The value of the weight of shock position α is defined as the maximum in the tip region, where a strong shock wave occurs. On the other hand, the weighted value of the pressure difference at the leading edge β is defined as large in the hub region, where a weak shock wave is generated. And in the Eq.(2), each DPL_k means the pressure difference of near leading edge, defined as the range from the leading edge to the 3% chord length of the profile.

Table.1 Details of k, α, and β

k	Span	Value	
		α_k	β_k
1	5%(Hub)	0	0.2
2	25%	0.1	0.8
3	50%(Mean)	0.2	0
4	75%	0.3	0
5	95%(Tip)	0.4	0

In addition to the Xs and DPL defined above, the efficiency at the design point ηd is also an objective function of the optimization system. The definition of ηd is shown in the Eq.(3). To optimize three objective functions simultaneously, MOGA, which is suitable for optimization with a large solution space, is applied as the optimization algorithm.

$$\eta_d = \frac{\left(Pt_2/Pt_1\right)^{\frac{\gamma-1}{\gamma}} - 1}{Tt_2/Tt_1 - 1} \tag{3}$$

CFD solver

The CFD solver for the system is the ANSYS-CFX10.0. At the inlet, span-wise distributions of the total pressure, total temperature, and flow angle are fixed. At the outlet, an area-averaged static pressure is fixed. The span-wise distribution of the static pressure at the outlet is calculated so as to satisfy the radial equilibrium. In the circumferential direction, a periodic boundary condition is imposed. The tip wall is assumed to stand stationary, and the hub wall is assumed to move with blades. A standard k-epsilon model is used as the turbulence model of the flow field.

The validation of the CFD solver is carried out by calculating the aerodynamic performance of the NASA Rotor 37, which is a highly-loaded transonic compressor blade. The specification is shown in table.2. Since the design information and detailed measurement data were provided by Reid and Moore (1978, 1980), it is generally used for the validation of CFD solvers for transonic compressor blades by such as Dunham (1998). The mesh size of the validation is approximately 450,000 elements including the tip clearance meshes.

Figs.6 to 8 show the results. Fig.6 is the comparison of the flow characteristics of pressure ratio and efficiency with the experimental data. Figs.7 and 8 are the comparisons of the Mach number contours at 90% span, and 50% span, respectively. In fig.6, the normalized mass flow rate is defined as the ratio of the mass flow rate of an operating point divided by that of the choke point. And in figs.7 and 8, the normalized mass flow rate is 0.98. Fig.6 shows the CFD solver underestimates both the pressure ratio and efficiency compared with the experiment, but the flow fields of the CFD solver show the good agreement with the experiment in figs.7 and 8. Since it is important for the system that the flow field such as the shock position can be predicted accurately, the CFD solver is able to be applied to the system.

Table.2 Specification of Rotor 37

Item	Unit	Value
Massflow	kg/s	20.96
Pressure ratio	-	2.106
Number of rotation	rpm	17188
Number of blade	-	36
Aspect ratio	-	1.19
Tip relative inlet Mach number	mm	1.48
Tip solidity	-	1.29
Tip clearance	mm	0.356

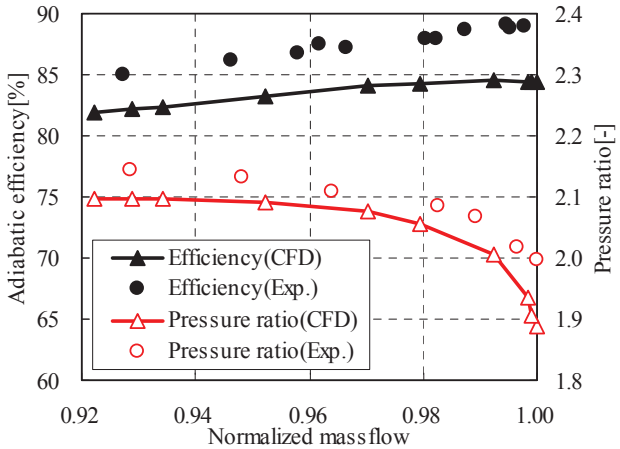

Fig.6 Comparison of the flow characteristics

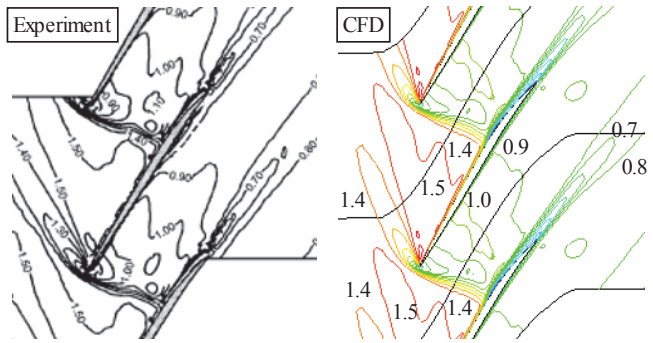

Fig.7 Comparisons of the Mach number contours at 90% span

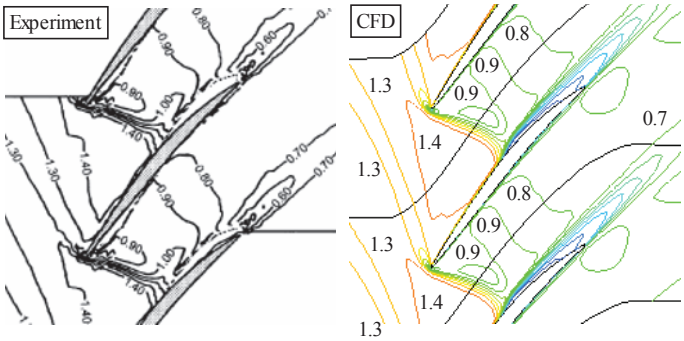

Fig.8 Comparisons of the Mach number contours at 50% span

Structural analysis

Fig.9 shows the conceptual diagram of the structural analysis. This system estimates primary stresses, maximum local stress, and natural frequency. As primary stresses, σ_c, centrifugal stress at hub, and σ_g, gas bending stress, are estimated. The criterion of the primary stress is that the summation of σ_c and σ_g is lower than the acceptable value of the blade.

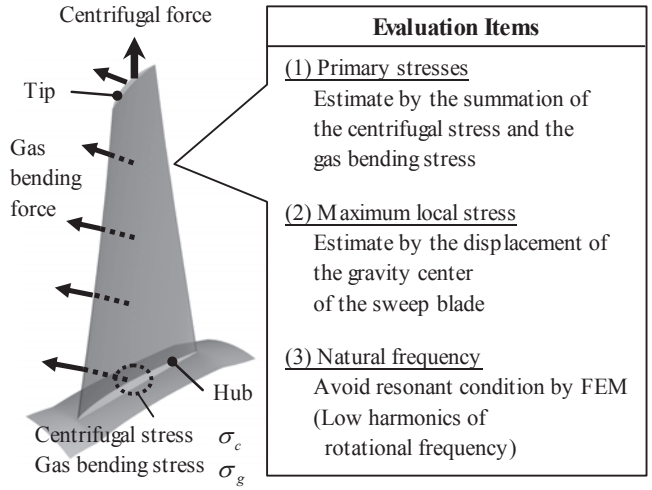

Fig.9 Conceptual diagram of the structural analysis

To estimate the maximum local stress, the relationship between the displacement of the gravity center of the sweep blade from the original blade and the increase of the maximum local stress is calculated in advance by the finite element method (FEM) analysis. In this system, the criterion of the local stress is the displacement of the gravity center. FEM analysis is also used for estimation of the natural frequency. All calculations are carried out with the ANSYS 11.0, and the mesh has a size of about 6600 elements. The blade is clamped at the hub, and disc effects are not taken into account. Calculated natural frequency is compared with the rotational frequency and low harmonics values of them to avoid resonant conditions.

TRANSONIC COMPRESSOR BLADE DESIGN RESULTS

Design conditions

Table.3 shows the configuration of the original blade. This blade is designed as the first stage rotor of an industrial gas turbine. Since the inlet Mach number of the tip region, which is more than 50% span, exceeds unity, a shock wave would be generated on the blade surface. Therefore, a shock loss reduction can be expected by applying the optimization system.

Fig.10 shows an example of calculation mesh. For calculations in the optimization system, a coarse mesh (approximately 150,000 elements) is used to reduce the total design time. For the off-design performance evaluation of the optimized blade, a fine mesh (approximately 300,000 elements) is used. In both calculation meshes, tip clearance is not modelled. However, as shown in the following, the flow field of the original blade at the design point by the calculation mesh is almost the same as that by the calculation mesh with tip clearance. Therefore, at least in this calculation condition, tip clearance has little effect on the optimization results.

Table.3 Configuration of the original blade

Item	Hub	Mean	Tip
Pressure ratio	1.41	1.32	1.37
Inlet Mach number	0.82	1.02	1.21
Solidity	1.59	1.30	1.14

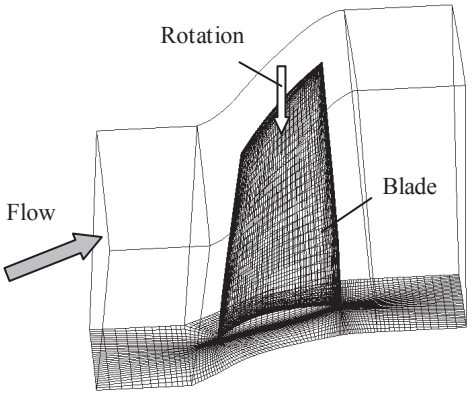

Fig.10 Example of calculation mesh (Fine mesh)

Table.4 shows the aerodynamic constraints of the optimization. The constraints are related to two conditions, that is, at the design point and at off-design points. The constraints related to the design point are the mass flow rate, pressure ratio, and average turning angle, which prevent reduction of the design performance and a big change of the velocity triangle. On the other hand, the constraints related to off-design points are Xs and DPL, defined previously, which prevent reduction of the performance near the stall point.

Table.4 Aerodynamic constraints of the optimization

Item		Description
Performance at design point	Mass flow rate	Higher than the original
	Pressure ratio	Higher than the original
	Average turning angle	Difference from the original is less than 1deg
Off-design performance	Pressure difference at leading edge	Less than the original
	Shock position	Downstream compared with the original

The optimization of the original blade is carried out for two conditions. The first one is the condition without estimations of the local stress from the displacement of the gravity center (case 1), and the other one is the condition with it (case 2). The acceptable value of the displacement in case 2 is 0.5% of the blade height H. Since there is no solution meeting the constraints, the criterion of the pressure ratio at the design point in case 2 is changed to 0.99 times its original value in Table.4. It should be noted that the solutions obtained by the case 1 may not satisfy the limit of the local stress. In other words, detailed FEM calculations for the solutions should be carried out before applying them as an actual compressor blade.

Optimization results

Figs.11 to 14 show the optimization results. Figs.11 and 13 show the relationship between DPL and Xs, and figs.12 and 14 show the relationship between Xs and ηd normalized by the efficiency of the original blade. In each figure, better solutions are located on the upper left or upper right. All figures imply that the Pareto solutions (shown as triangles) are obtained by the optimization. In the optimization, a PC cluster with 4 CPUs (CPU : Dual Core 2.2GHz, memory : 8GB) are used. The total calculation time is about two weeks, while the calculation time for each solution is from 15 to 20 minutes.

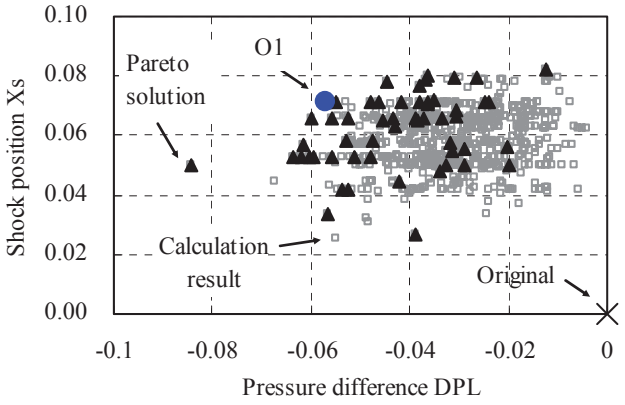

Fig.11 Relationship between DPL and Xs (case1)

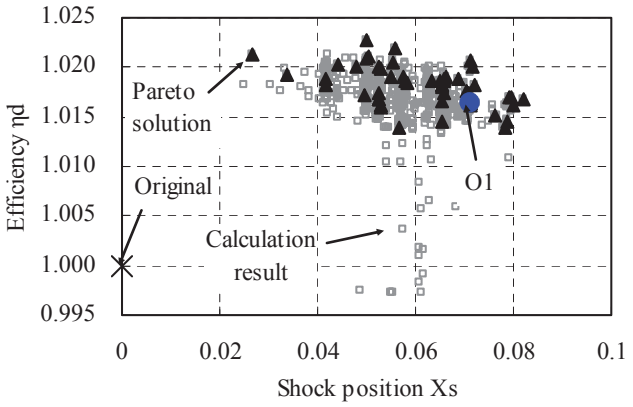

Fig.12 Relationship between Xs and ηd (case1)

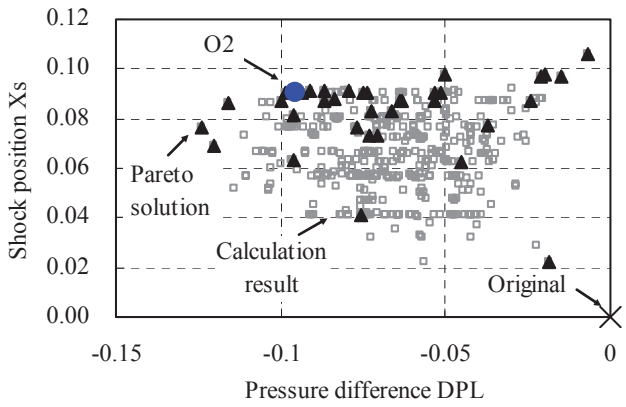

Fig.13 Relationship between DPL and Xs (case2)

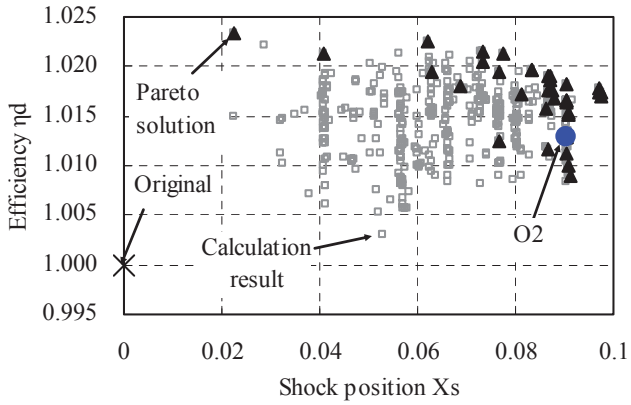

Fig.14 Relationship between Xs and ηd (case2)

Off-design performance calculations are done for one of the Pareto solutions in each of the figures; they are designated O1 (for case 1), and O2 (for case 2). They are selected because both Xs and DPL are improved from the original values. To validate the optimization method, another performance calculation is done for a blade optimized by the method just with the objective function of ηd (designated O3) as the reference.

Table.5 summarizes the off-design performances, and figs.15 and 16 show the flow characteristics of the pressure ratio and efficiency, respectively. All results are normalized by the results of the original blade at the design point. The stall point is defined as the point at which the calculation first fails to converge when the operating pressure ratio is increased. And all the calculation results at the design point are obtained by using the boundary condition of the original blade.

Those results imply that O3 has the best performance at the design point while the pressure ratio at the stall point is much lower than the original blade. Compared with O3, O1 and O2 improve the pressure ratio at the stall point, the mass flow rate at the choke point, and efficiencies at all operating points from the original blade, though the improvement of efficiency at the design point is about 1.5%, which is lower than for O3. By comparison among blades, the optimization method proposed in this paper can provide the blades which improve off-design performance from the original blade. The comparison between O1 and O2 also shows the displacement limit of the blade center of gravity has only a little impact on the improvement because the performance of O1 is only slightly better than that of O2.

However, the Pareto solutions obtained by the proposed method do not always show the off-design performance improvement. So off-design performance calculations are conducted for some Pareto solutions of case 1, where both Xs and DPL are improved from the original values like O1. The results implies that the selected

solutions have the higher pressure ratio and efficiency at the design point, choke point, and stall point though the mass flow rates at the stall point sometimes increase from the original value. Therefore, the proposed method are likely to provide the Pareto solutions which improve the off-design performance at least by selecting the solutions whose Xs and DPL are better than the original blade.

Table.5 Summary of off-design performances

Item		Original	Optimized		
			O1	O2	O3
Design point	Mass flow	1.000	1.009	1.002	1.023
	Pressure ratio	1.000	1.003	0.994	1.016
	Efficiency	1.000	1.016	1.015	1.041
Stall point	Mass flow	0.904	0.898	0.896	1.002
	Pressure ratio	1.149	1.171	1.168	1.058
	Efficiency	0.986	0.988	0.987	1.035
Choke point	Mass flow	1.000	1.009	1.003	1.025
	Pressure ratio	0.904	0.908	0.900	0.924
	Efficiency	0.931	0.947	0.941	0.980

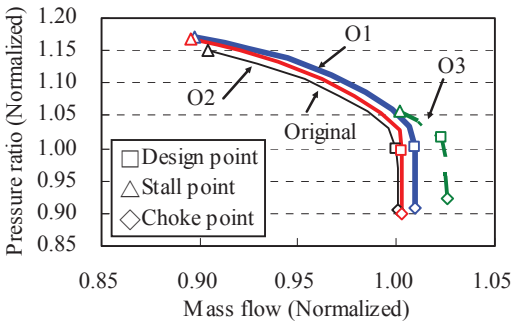

Fig.15 Flow characteristics of pressure ratio

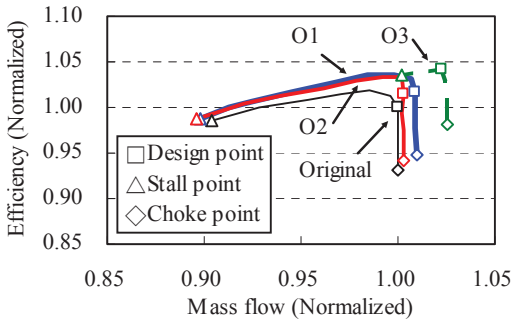

Fig.16 Flow characteristics of efficiency

Relationship between aerodynamic performance and blade shape

Figs.17 to 19 compare the hub, mean, and tip profiles, figs.20 to 22 compare those profiles on suction surface, and fig.23 compares the stacking lines. In the figures, profiles are normalized by the chord length C.

Those figures imply that the profile of O1 do not have any big difference from O2 except for the thickness of hub profile at the downstream. Compared with the original blade, O1 and O2 have higher stagger angles at the hub and for the mean, and their upstream profile changes are smaller on the suction surface for the mean and at the tip. On the other hand, O3 has a lower stagger angle than the original blade at the hub. And its upstream profile change on suction surface for the mean is smaller than those of O1 and O2. Unlike the profiles, the stacking line of O1 is different from that of O2. O1 is a forward sweep blade, in which the stacking line is shifted to the upstream direction and the shift at the tip region is bigger than at the hub region, while O2 has only a little sweep. The stacking line of O3 is an S-shaped curve, which shifts to the downstream direction around the mean region and to the upstream direction at the tip region. Compared with the original blade and O2, the mass flow rates of the choke point of O1 and O3 are improved. To explain the reason, fig.24 shows the comparison of the cross-sectional area distributions. In fig.24, the cross-sectional area is normalized by that of the inlet. This figure shows that the minimum value of the cross-sectional area of O1 and O3 is bigger than the original blade and O2. Because of the increase of the minimum value of the cross-sectional area of the blade, O1 and O3 show the better choke mass flow rate.

Fig.25 shows the comparison of the span-wise distribution of efficiency. The efficiencies of O1, O2, and O3 are better than the original blade, especially from the mean region to the tip region, where stronger shock waves exist. The result implies that O1, O2, and O3 achieve the reduction of shock by changes of blade shapes.

Figs.26 to 28 are the comparisons of the blade surface Mach number distribution at design point, fig.29 is the comparison of the Mach number contours on the suction surface. In figs. 26 to 29, the calculation result of the original blade considering the tip clearance is also shown. These figures show that the flow field calculated by the calculation mesh with the tip clearance is almost the same as that by the calculation mesh without tip clearance. Therefore, at least in this calculation condition, tip clearance has little effect on the optimization results.

These figures also show that the peak Mach number of O3 is lower than that of the original blade whereas the shock position at 75% span is shifted to the upstream direction. This shift of shock position and the lower stagger angle at the hub contribute to the off-design performance degradation when the operating pressure ratio is increased. The shift is mainly due to the fact that O3 is designed to reduce the shock loss only at the design point by alleviating the change of the cross-sectional area of the flow passage using the S-shaped stacking line.

On the other hand, the peak Mach number of O1 and O2 for the mean is lower than the original blade and the shock position at 75% span is shifted to the downstream direction, though the decrease of the peak Mach number is lower than for O3. The downstream shift of the shock position of O1 and O2 is mainly due to the smaller upstream profile changes on the suction surface for the mean and tip, because they move the position of the maximum value on suction surface to the downstream direction. Since they also control the sharp velocity increase on the suction surface, there is a reduction of the peak Mach number for the mean, where the stagger angle is higher and the turning angle is lower than original blade values.

Comparison between O1 and O2 shows that there is little difference in the shock position at the tip and for the mean while the peak Mach number of O1 is a little lower than O2. This result implies that the difference of the stacking lines has less effect on the flow field and aerodynamic performance at the tip and for the mean than that of the profiles at least in this optimization case, because the mean and tip profiles of O1 are almost the same as those of O2 in spite of the difference of their stacking lines. On the other hand, fig.29 shows that O2 has a larger separation area around the 25% span, because the shock position of O2 is located more downstream than that of O1 and the shock interacts with the boundary layer on the blade suction surface. The downstream shift of the shock position of O2 is caused by the thicker hub profile at the downstream. Therefore, the efficiency of O2 around the 25% span is lower than that of O1.

To summarize the results, the off-design performance improvement of O1 and O2 is achieved by the reduction of the peak Mach number and the downstream shift of the shock position.

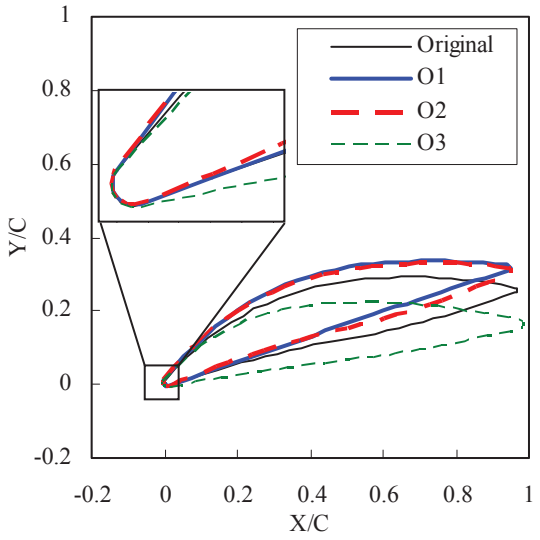

Fig.17 Comparison of hub profile

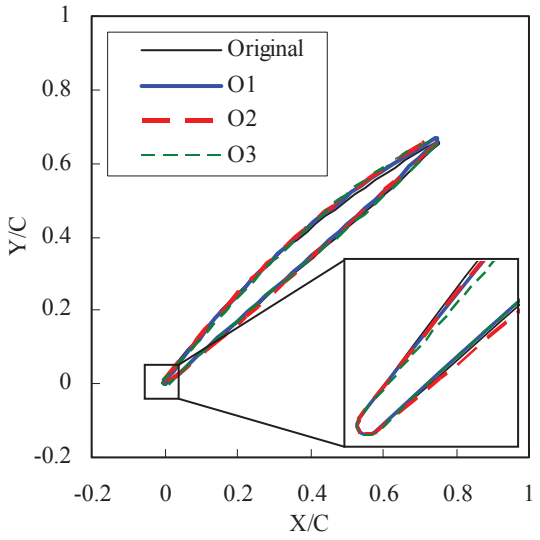

Fig.18 Comparison of mean profile

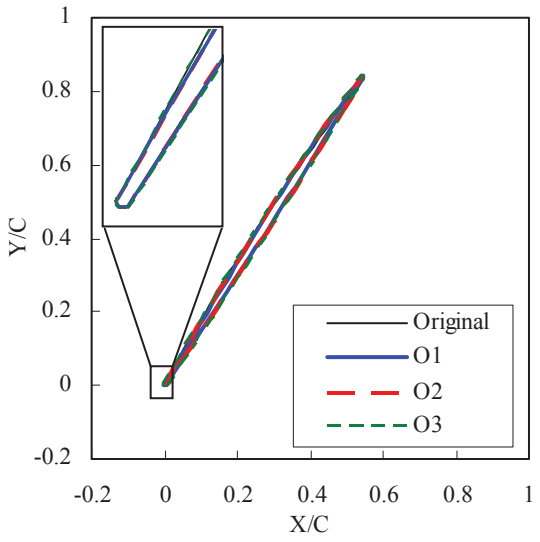

Fig.19 Comparison of tip profile

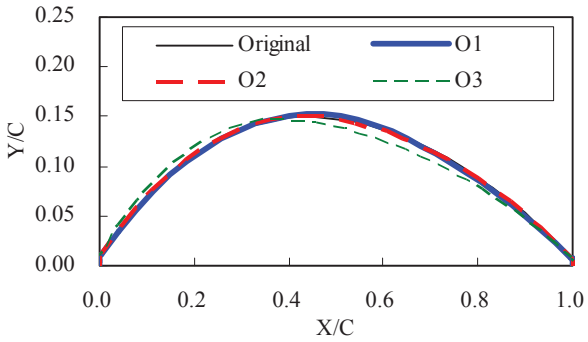

Fig.20 Comparison of hub profile on suction surface

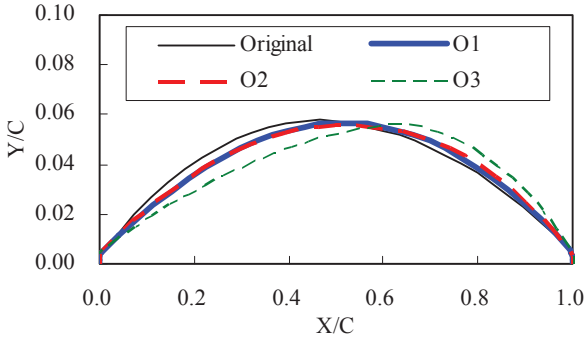

Fig.21 Comparison of mean profile on suction surface

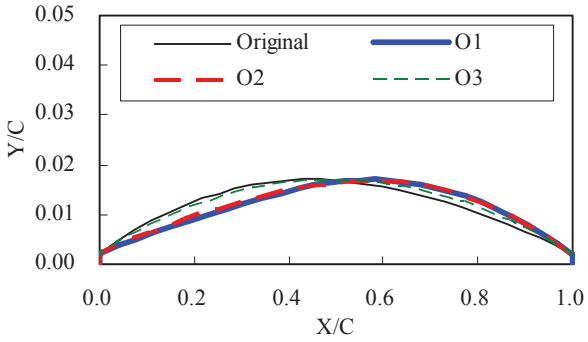

Fig.22 Comparison of tip profile on suction surface

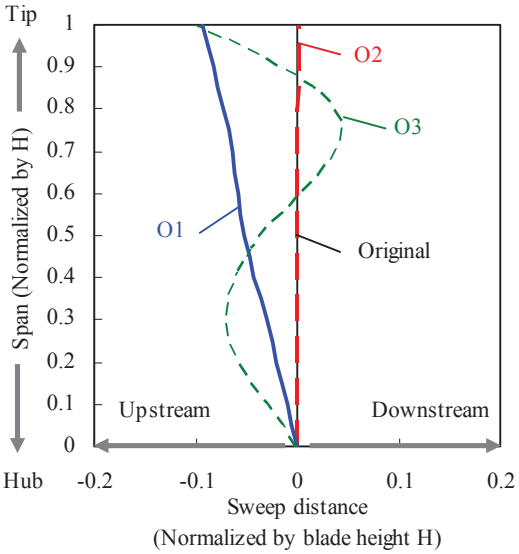

Fig.23 Comparison of the stacking lines

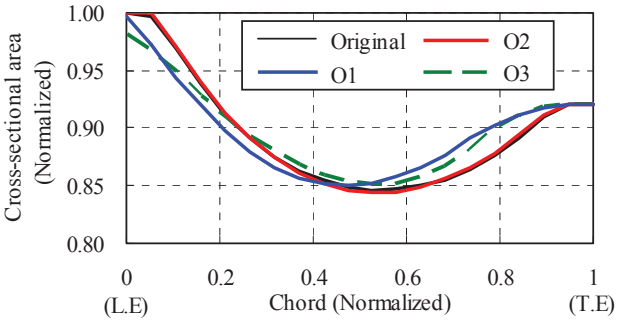

Fig.24 Comparison of the cross-sectional area distributions

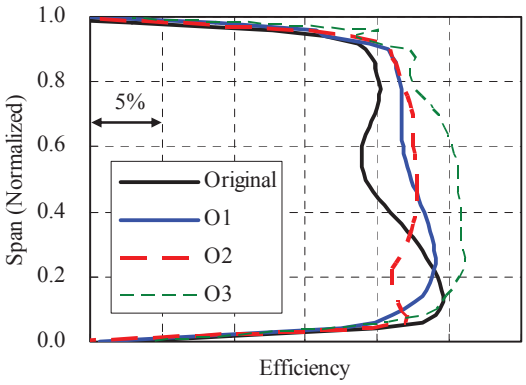

Fig.25 Comparison of the span-wise distribution of efficiency at design point

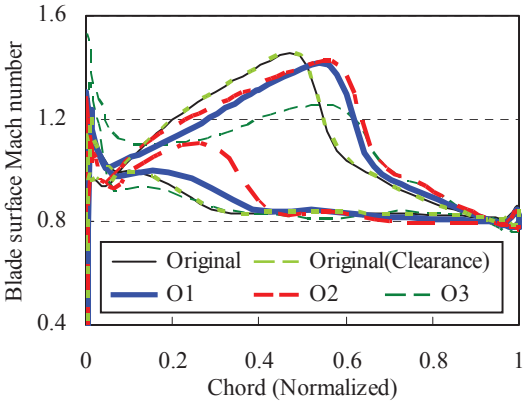

Fig.26 Comparison of the blade surface Mach number distribution at design point (Mean)

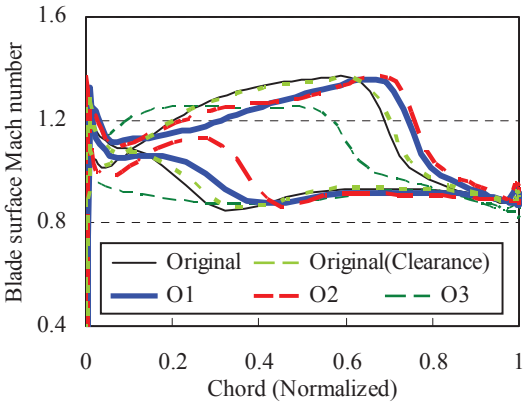

Fig.27 Comparison of the blade surface Mach number distribution at design point (75% span)

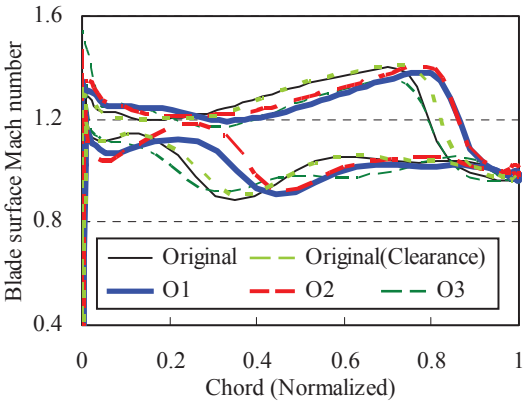

Fig.28 Comparison of the blade surface Mach number distribution at design point (Tip)

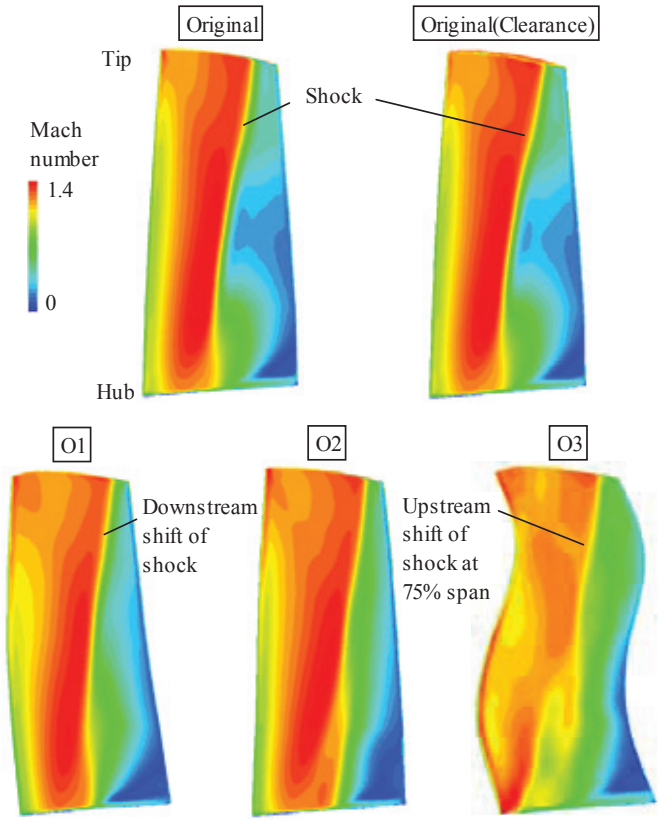

Fig.29 Comparison of the Mach number contours on suction surface at design point

CONCLUSIONS

A 3D blade design method to optimize the aerodynamic performance at the design point and off-design points by only one prediction at the design point was developed. This method was applied in aerodynamic design of a blade (original blade), whose specifications were almost the same as the first stage rotor of a conventional gas turbine axial compressor. The optimization of the original blade is carried out for two conditions. In each condition, one of the Pareto solutions (O1 and O2) was selected, and the aerodynamic performance was compared with that of a blade optimized only at the design point (O3). The results showed the following.

(1) The blades optimized by the objective function with Xs and DPL (O1 and O2) have better overall performance characteristics than the original blade except for slightly

relaxing the constraint on pressure ratio O2 at its nominal design point, and the improvements of efficiency at the design point were about 1.5%. The improvements of efficiency at the design point and the pressure ratio at the stall point were caused by the reduction of the peak Mach number for the mean and the downstream shift of the shock position.

(2) The blade optimized by the objective function just with ηd (O3) showed the best performance at the design point while the pressure ratio at the stall point was much lower than the original blade. Comparing O1, O2, and O3 showed that the optimization method proposed in this paper were likely to provide the Pareto solutions which improved the off-design performance.

(3) The comparison between O1 and O2 also showed that there is little difference in the shock position at the tip and for the mean. This result implies that the difference of the stacking lines has less effect on the flow field and aerodynamic performance at the tip and for the mean than that of the profiles at least in this optimization case.

REFERENCES

Bonaiuti, D., Pitigala, A., Zangeneh, M., and Li, Y., 2007, "Redesign of a Transonic Compressor Rotor by means of a Three-Dimensional Inverse Design Method : A Parametric Study", *Proceedings of ASME Turbo Expo,* ASME GT 2007-27846.

Denton, J.D. and Xu, L., 2002, "The Effects of Lean and Sweep on Transonic Fan Performance", *Proceedings of ASME Turbo Expo,* GT 2002-30327.

Dunham, J., 1998, "CFD Validation for Propulsion System Components", AGARD Advisory Report 355.

Iwatani, J., Ito, E., Owaki, T., Nagai, N., and Seki, N., 2007, "Development of Compressor Transonic Rotor for Next Generation Gas Turbine", *Proceedings of IGTC2007 Tokyo,* TS-051.

Li, H.D., He, L., Li, Y.S., and Wells, R., 2006, "Blading Aerodynamics Design Optimization with Mechanical and Aeromechanical Constraints", *Proceedings of ASME Turbo Expo,* GT 2006-90503.

Luo, C., Song, L., Li, J., and Feng, Z., 2009, "Multiobjective Optimization Approach to Multidiciplinary Design of a Three-Dimensional Transonic Compressor Blade", *Proceedings of ASME Turbo Expo,* GT 2009-59982.

Moore, R. D., Reid, L., 1980, "Performance of Single-Stage Axial Flow Transonic Compressor with Rotor and Stator Aspect Ratios of 1.19 and 1.26, Respectively, and with Design Pressure Ratio of 2.05", *NASA Technical Paper,* TP1659.

Reid, L., Moore, R. D., 1978, "Design and Overall Performance of Four Highly loaded, High-speed Inlet Stages for an Advanced High-Pressure-Ratio Core Compressor", *NASA Technical Paper,* TP1337.

Zheng, R., Xiang, J., and Sun, J., 2010, "Blade Geometry Optimization for Axial Flow Compressor", *Proceedings of ASME Turbo Expo,* GT 2010-22229.